

Tunable magnetic field effects on the near-field radiative heat transfer in planar three-body systemsLei Qu,^{1,2} Edwin Moncada-Villa,^{3,*} Jie-Long Fang,^{1,2} Yong Zhang,^{1,2} and Hong-Liang Yi^{1,2,†}¹*School of Energy Science and Engineering, Harbin Institute of Technology, Harbin 150001, People's Republic of China*²*Key Laboratory of Aerospace Thermophysics, Ministry of Industry and Information Technology, Harbin 150001, People's Republic of China*³*Escuela de Física, Universidad Pedagógica y Tecnológica de Colombia, Avenida Central del Norte 39-115, Tunja, Colombia*

(Received 12 August 2022; revised 18 April 2023; accepted 25 April 2023; published 12 May 2023)

Recently, the application of an external magnetic field to actively control the near-field radiative heat transfer (NFRHT) has emerged as an appealing and promising technique. Most prior studies have shown that the externally static magnetic field can only reduce the near-field flux transferred between two planar magneto-optical (MO) structures, yet so far the thermomagnetic effect in many-body systems consisting of such structures has not been revealed. Here, we investigate how the presence of an external static magnetic field modifies the nanoscale heat transfer in a MO many-body configuration comprising three noncontact slabs made of n -doped InSb. To this end, we first generalize a general Green's function approach for the calculation of the radiative energy transfer in many-body planar geometries composed of materials with complex optical anisotropy. Based on this approach, we show that the presence of a third MO body allows for either the reduction or even the enhancement of the NFRHT between MO slabs by applying external magnetic fields, which depends on the interplay between the zero-field surface waves and propagating hyperbolic modes induced by fields. Our study not only deepens the understanding of the active control of the nanoscale heat transfer via the applied magnetic field, but also paves the way for the magnetic regulation of energy fluxes in complex macroscopic many-body systems.

DOI: [10.1103/PhysRevB.107.205405](https://doi.org/10.1103/PhysRevB.107.205405)**I. INTRODUCTION**

Two objects held at different temperatures and separated by a vacuum gap transfer heat via electromagnetic waves. As is well known, this radiative heat transfer (RHT) cannot exceed the blackbody limit set by the Stefan-Boltzmann law if the separation between objects is greater than the thermal wavelength. Nevertheless, when objects are in close proximity to each other, at a distance below this characteristic length, an additional contribution, known as the near-field radiative heat transfer (NFRHT), originating from the evanescent field of surface waves, can overcome by several orders of magnitude the prediction of Planck's blackbody theory [1–6]. Such a new contribution to the RHT has triggered the research of functional devices for modern energy technologies, such as thermophotovoltaics [7–10], thermal lithography [11], heat-assisted magnetic recording [12], and scanning thermal microscopy [13].

The past decades have seen a growth of interest in modifying the NFRHT by the engineering of photonic structures as well as the choice of materials whose optical properties are optimal for the NFRHT [14–19]. In parallel, an important problem is the active control and modulation of the NFRHT, for which many innovative strategies have been proposed [20–26]. One currently appealing and promising scenario is the use of an external static magnetic field to ac-

tively control near-field thermal radiation of magneto-optical (MO) media [27]. Special attention has been devoted to magnetic semiconductors such as InSb or Si due to their unique optical properties sensitive to the action of a magnetic field, leading to strong MO activities in the infrared (highly relevant for thermal radiation). This strategy for controlling the NFRHT was proposed by Moncada-Villa *et al.* in Ref. [23], where it was shown theoretically that the RHT in the near-field regime between two identical MO planar slabs of n -doped InSb is always reduced by the application of a static magnetic field. Such a field-induced reduction is a consequence of the fundamental change of TM evanescent modes under the action of magnetic fields, i.e., the replacement of surface polariton modes (evanescent inside slabs as well as in vacuum), which dominate the zero-field heat transfer, by field-induced hyperbolic modes (propagating inside slabs but evanescent in vacuum) which have a lower tunneling probability. Similar magnetic field effects were subsequently observed in several other symmetric configurations, such as two identical MO nanospheres [28,29] or magnetophotonic crystals [30,31], where the presence of external fields still only suppresses the transfer of near-field energy fluxes. These results make one wonder whether there exist MO systems in which the applied magnetic field is capable of enhancing the NFRHT. However, so far, this possibility have been reported only for the asymmetric configurations, as a semi-infinite InSb separated by a vacuum gap from a different material such as gold [32] or drift-current-biased graphene [33]. The field-induced near-field enhancement in the former nonsymmetric case results from an increasing contribution from TE modes

*edwin.moncada@uptc.edu.co

†yihongliang@hit.edu.cn

that overcomes the deleterious effect of magnetic fields upon TM modes due to the appearance of hyperbolic modes, while, in the latter case, the enhancement behavior is related to the interplay between the nonreciprocal photon occupation number from graphene and surface modes of InSb.

The above-mentioned studies on magnetic field effects upon the NFRHT are confined to MO two-body systems (involving only two dissimilar temperatures). However, in an experimental setup, the RHT often takes place between three or even more bodies, in analogy to standard many-body problems in condensed matter physics [34,35], atomic physics [36], etc. In the context of the NFRHT, many-body systems consisting of more than two thermal emitters that are primarily small spheres (usually considered as dipoles) [37–42] or macroscopic planar slabs [43–49] have attracted wide attention during recent years. In these systems, plenty of novel physical phenomena with no analogs in two-body systems have been demonstrated using different theoretical frameworks, e.g., the many-body radiative transfer theory [37], scattering method [50,51], and trace formulas [52–54], to mention just a few. These demonstrations enable the tailoring of functional devices for thermal management following the operating principle of electronic devices, as the near-field thermal transistor attests [44]. More importantly, in many-body systems consisting of MO nanospheres at near-field separations, one has predicted some very peculiar many-body phenomena, including persistent heat current in thermal equilibrium [39], the thermal Hall effect [55], the giant thermal magnetoresistance [56], and so on [57], by applying a static magnetic field. In spite of these remarkable advances, the magnetic field effect upon the NFRHT in a many-body planar configuration composed of MO materials remains unexplored. It is worth noting that MO media, like magnetic semiconductors, in the magnetic field are optically anisotropic and nonreciprocal and their permittivity tensor has complex off-diagonal components, rendering many-body planar geometries comprising such materials fundamentally different from almost all reported ones that involve only isotropic or uniaxial materials satisfying Lorentz reciprocity [43–48,51,58–60]. In this regard, investigating the magnetic field dependence of the heat transfer in compact MO many-slab systems would be instructive for developing magnetically thermal functional devices and meaningful for the NFRHT community.

In this work, we examine theoretically how the presence of an external static magnetic field influences the near-field heat transfer in a MO many-body system, consisting of three noncontact, parallel slabs of n -doped InSb, with a symmetric arrangement [Fig. 1]. A general Green's function approach, which is generalized from the formalism proposed in Ref. [61] and suitable for describing the RHT in many-body planar configurations made of optically anisotropic materials, allows us to precisely calculate the flux transferred in the considered system. We demonstrate that, under certain choices of the geometrical and thermal parameters, the presence of the intermediate MO slab makes it possible to either reduce or enhance the NFRHT in the symmetric MO configuration by applying a magnetic field, in stark contrast to the previously mentioned

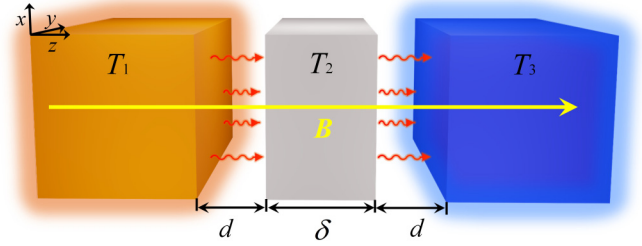


FIG. 1. Schematic representation of three parallel slabs made of n -doped InSb in the presence of an external static magnetic field parallel to the transfer direction of fluxes. An intermediate slab with thickness δ is placed in between the outermost slabs, and separated by vacuum gaps of size d .

magnetic field behaviors appearing in two-body cases [23,28–33]. Such a tunable magnetic field effect is due to the interplay between the zero-field surface modes and the field-induced propagating hyperbolic modes. Our findings enrich and enhance the understanding concerning the use of external fields to actively control the heat transfer at the nanoscale.

The remainder of this paper is organized as follows. In Sec. II, we present a description of the system under consideration. In Sec. III, we generalize the Green's function approach for the calculation of the RHT in many-body planar configurations comprising materials with any type of optical anisotropy. Section IV is devoted to the analysis of the underlying mechanisms behind the magnetic-field-induced reduction/enhancement of the NFRHT in MO three-body systems near thermal equilibrium, and, in Sec. V we briefly discuss the magnetic field effect upon the radiative energy flux under a steady-state situation. Our main results are summarized in Sec. VI.

II. PHYSICAL SYSTEM UNDER STUDY

The goal of this paper is the calculation of the NFRHT in a system out of thermal equilibrium, consisting of three noncontact planar slabs made of MO n -doped InSb, in the presence of an external static magnetic field \mathbf{B} , as depicted in Fig. 1. The outermost slabs 1 and 3, assumed as semi-infinite, are held at temperatures T_1 and T_3 ($T_1 > T_3$), respectively, whereas slab 2 placed between them has a temperature T_2 and a thickness δ . This slab is separated by vacuum gaps of size d from the outermost slabs. From now on, we assume that the orientation of the applied magnetic field is perpendicular to the surface of the slabs, i.e., $\mathbf{B} = B\hat{z}$. It should be mentioned that the rotation of the field orientation does not radically change the radiation property of planar InSb [32]. In the presence of an external field oriented as $\mathbf{B} = B\hat{z}$, InSb exhibits an optical anisotropy described by the following dielectric permittivity tensor [62],

$$\hat{\epsilon}_{\text{InSb}} = \begin{bmatrix} \epsilon_1 & -i\epsilon_2 & 0 \\ i\epsilon_2 & \epsilon_1 & 0 \\ 0 & 0 & \epsilon_3 \end{bmatrix}, \quad (1)$$

where

$$\begin{aligned}\varepsilon_1(B) &= \varepsilon_\infty \left\{ 1 + \frac{\omega_L^2 - \omega_T^2}{\omega_T^2 - \omega^2 - i\Gamma\omega} + \frac{\omega_p^2(\omega + i\gamma)}{\omega[\omega_c^2 - (\omega + i\gamma)^2]} \right\}, \\ \varepsilon_2(B) &= \frac{\varepsilon_\infty \omega_p^2 \omega_c}{\omega[(\omega + i\gamma)^2 - \omega_c^2]}, \\ \varepsilon_3 &= \varepsilon_\infty \left[1 + \frac{\omega_L^2 - \omega_T^2}{\omega_T^2 - \omega^2 - i\Gamma\omega} - \frac{\omega_p^2}{\omega(\omega + i\gamma)} \right].\end{aligned}\quad (2)$$

Here, $\varepsilon_\infty = 15.7$ is the high frequency permittivity, $\omega_L = 3.62 \times 10^{13} \text{ rad s}^{-1}$ ($\omega_T = 3.39 \times 10^{13} \text{ rad s}^{-1}$) is the longitudinal (transverse) phonon frequency, $\omega_p = 3.14 \times 10^{13} \text{ rad s}^{-1}$ is the plasma frequency, and $\Gamma = 5.65 \times 10^{11} \text{ rad s}^{-1}$ ($\gamma = 3.39 \times 10^{12} \text{ rad s}^{-1}$) is the phonon (free carrier) damping constants. The effect of the magnetic field is expressed by cyclotron frequency $\omega_c = eB/m^*$, where $m^* = 1.99 \times 10^{-32} \text{ kg}$ is the effective mass corresponding to a doping level of $1.07 \times 10^{17} \text{ cm}^{-3}$. It is worth mentioning that Eq. (2) does not account for the nonlocal effect [63].

In the absence of magnetic fields, $\varepsilon_1 = \varepsilon_3$ and $\varepsilon_2 = 0$, so InSb is optically isotropic. In this case, the interface between the InSb slab and vacuum can support either surface plasmon polaritons (SPPs) at the frequencies below the surface plasmon frequency $\omega_{\text{spp}} = \omega_p/\sqrt{2}$ or surface phonon polaritons (SPhPs) in the reststrahlen band $\omega_L < \omega < \omega_T$ [62]. These modes are characterized by an evanescent field inside both InSb and vacuum, with a large component of the wave vector parallel to the interfaces, thus favoring a strong transfer of heat fluxes. When the magnetic field is turned on, MO effects are induced due to the generation of the complex off-diagonal elements ε_2 , and in certain frequency regions a different kind of electromagnetic mode emerges. These modes are referred to as hyperbolic modes (HMs), and are classified as type I hyperbolic modes (HMI) with $\varepsilon_1 > 0$ and $\varepsilon_3 < 0$ and type II (HMII) with $\varepsilon_1 < 0$ and $\varepsilon_3 > 0$, as discussed in Ref. [23]. These HMs are propagating inside InSb but evanescent in vacuum, and their components of the wave vector parallel to the interfaces is much smaller than those of the surface waves, so that they are less effective in transferring heat [23,31]. This is the fundamental reason for the reduced NFRHT between two identical InSb slabs under the application of magnetic fields.

We focus on the analysis of the net heat flux, φ_3 , received by the cold body, i.e., slab 3. Considering the stable nonreciprocity of InSb in the magnetic field [37,56], the net heat flux φ_3 in the considered system must be calculated by the following Landauer-like expression [56],

$$\begin{aligned}\varphi_3 &= \int_0^\infty \frac{d\omega}{2\pi} \int \frac{d\mathbf{k}}{(2\pi)^2} \sum_{j=1,2} [\Theta_j(\omega, T_j) \mathcal{T}_{j \rightarrow 3}(\mathbf{k}, \omega) \\ &\quad - \Theta_3(\omega, T_3) \mathcal{T}_{3 \rightarrow j}(\mathbf{k}, \omega)],\end{aligned}\quad (3)$$

where index $j = 1, 2$; $\Theta_j(\omega, T_j) = \hbar\omega/[exp(\hbar\omega/k_B T_j) - 1]$ is the mean energy of photons with frequency ω ; $\mathbf{k} = (k_x, k_y)$ is the component of the wave vector parallel to the interface; and $\mathcal{T}_{j \rightarrow 3}$ ($\mathcal{T}_{3 \rightarrow j}$) denotes the transmission probability for the thermal photons coming from slab j to slab 3 (slab 3 to slab j), whose calculation will be described in the next section.

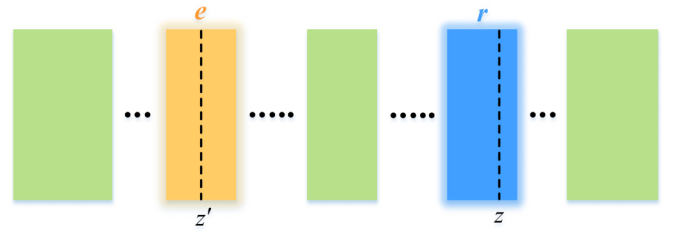


FIG. 2. Schematics of the system comprising any number of layers (bodies) that may have different thicknesses and temperatures. Thermal emission of fluctuating currents contained in the z' plane in layer e is absorbed by the z plane in the receiving layer r .

III. THEORETICAL APPROACH

As mentioned in the Introduction, almost all previous studies on the NFRHT in many-body planar systems only involve isotropic or uniaxial materials with the optical axis parallel to the heat transfer direction. In such systems, the photonic transmission probability is usually calculated using the analytical formula derived from the scattering approach [43,50,51]. This formula, however, fails to obtain the transmission probability in many-body systems containing complex anisotropic materials of which the permittivity tensor has off-diagonal components that give rise to polarization conversion [23,25].

Since thermal radiation stems from random fluctuating current sources, directly implementing the volume integration over all these sources is a very effective method, which has been extensively employed to investigate the NFRHT in different geometries, mainly involving finite objects (e.g., spheres [64,65] and even irregular shapes [66,67]) and infinite ones (e.g., layered structures [61,68] and period gratings [69]). In such an approach, the thermal radiation fields are linked to the fluctuating current sources via the electric and magnetic Green's functions. For layered structures, Francoeur *et al.* [61] first presented a Green's function formalism for the description of their RHT, where each layer (i.e., each body) may have dissimilar temperatures, enabling the calculation of the transmission probability between any two layers (bodies). In addition, it allows one to trace the radiative energy flux at any position in considered layered systems, which is unattainable for the scattering approach [43,50,51]. Despite its advantage relative to the scattering approach, this formalism based on the solution of Green's functions is still only applicable to materials that are isotropic or uniaxial anisotropic up to now. In what follows, we shall generalize it to the case where layered systems are made of complex anisotropic materials.

Let us consider a system consisting of multiple layers stacked in the z direction and infinite along the x and y directions, as sketched in Fig. 2. These layers may have different thicknesses and temperatures, and be made of materials with optical anisotropy described by a permittivity tensor $\hat{\varepsilon}$. As a concrete example, we consider the situation where the radiative flux is transferred from the emitting layer e to the receiving layer r . In order to determine the photonic transmission probability between them, the one at the two boundaries of layer r must be known first. For this purpose, we now calculate the flux at the arbitrary position z within layer r , originating from the fluctuating current sources within layer

e , given by the z component of the Poynting vector,

$$\varphi_{e \rightarrow z}(\mathbf{r}, t) = S(\mathbf{r}, z, t) = \hat{\mathbf{z}} \cdot \langle \mathbf{E}(\mathbf{r}, z, t) \times \mathbf{H}(\mathbf{r}, z, t) \rangle, \quad (4)$$

where $\langle \dots \rangle$ denotes the ensemble average, $\mathbf{E}(\mathbf{r}, z, t)$ and $\mathbf{H}(\mathbf{r}, z, t)$ are the electric and magnetic fields, and \mathbf{r} and t denote the in-plane coordinate and time, respectively. Using the Fourier transform in time and space, respectively, defined as $f(t) = \text{Re} \int_0^\infty d\omega f(\omega) e^{-i\omega t}$ and $f(\mathbf{r}) = \int \frac{d\mathbf{k}}{(2\pi)^2} f(\mathbf{k}) e^{i\mathbf{k} \cdot \mathbf{r}}$, Eq. (4) can be rewritten as

$$S(z) = \frac{1}{2} \int_0^\infty d\omega \int \frac{d\mathbf{k}}{(2\pi)^4} \text{Re} \{ \hat{\mathbf{z}} \cdot \langle \mathbf{E}(\mathbf{k}, z, \omega) \times \mathbf{H}^*(\mathbf{k}, z, \omega) \rangle \}. \quad (5)$$

For the convenience of calculations, we recast Eq. (5) into the following form:

$$S(z) = \frac{1}{2} \int_0^\infty d\omega \int \frac{d\mathbf{k}}{(2\pi)^4} \text{Re} \{ \text{Tr} [\hat{\Gamma} \langle \mathbf{E}(\mathbf{k}, z, \omega) \mathbf{H}(\mathbf{k}, z, \omega)^* \rangle] \}. \quad (6)$$

Here, the matrix $\hat{\Gamma} = \begin{bmatrix} 0 & -1 & 0 \\ 1 & 0 & 0 \\ 0 & 0 & 0 \end{bmatrix}$, and $\langle \mathbf{E} \mathbf{H}^* \rangle = \langle \mathbf{E}_\alpha \mathbf{H}_\beta^* \rangle$,

where α and β represent the Cartesian components. The thermally generated electric and magnetic fields in this equation can be solved by the sum of the contributions from the fluctuating current sources, $\mathbf{J}(\mathbf{k}, z', \omega)$, at all z' planes within layer e as

$$\mathbf{E}(\mathbf{k}, z, \omega) = \int_{z'} \hat{G}_E(\mathbf{k}, z, z', \omega) \mathbf{J}(\mathbf{k}, z', \omega), \quad (7)$$

$$\mathbf{H}(\mathbf{k}, z, \omega) = \int_{z'} \hat{G}_H(\mathbf{k}, z, z', \omega) \mathbf{J}(\mathbf{k}, z', \omega), \quad (8)$$

where \hat{G}_E and \hat{G}_H are the electric and magnetic Green's functions, which connect the emitting sources in a plane located at position z' in the emitting layer e , with the absorbing plane at position z in the receiving layer r . We note that the Green's functions given here differ from those in Ref. [61], and we employ a scattering matrix formalism [70] to accurately calculate these functions (see Supplemental Material [71] for details of the derivation).

From Eqs. (6)–(8) it is clear that the heat flux calculation involves the ensemble average of the spatial correlation function of \mathbf{J} within layer e , which can be given by the fluctuation-dissipation theorem [2],

$$\begin{aligned} & \langle \mathbf{J}(\mathbf{k}, z, \omega) \mathbf{J}^\dagger(\mathbf{k}', z', \omega) \rangle \\ &= (2\pi)^2 \frac{4}{\pi} \omega \varepsilon_0 \Theta(\omega, T_e) \frac{\hat{\varepsilon}_e - \hat{\varepsilon}_e^\dagger}{2i} \delta(\mathbf{k} - \mathbf{k}') \delta(z - z'), \end{aligned} \quad (9)$$

where T_e and $\hat{\varepsilon}_e$ are, respectively, the temperature and the permittivity tensor of the emitting layer e .

Plugging Eqs. (7)–(9) into Eq. (6), we obtain the following expression for the radiative heat flux at position z within the receiving layer r :

$$\begin{aligned} S(z) &= \int_0^\infty \frac{d\omega}{2\pi} \int \frac{d\mathbf{k}}{(2\pi)^2} 4\omega \varepsilon_0 \Theta(\omega, T) \int_{z'} \text{Re} \\ &\times \left\{ \text{Tr} \left[\hat{\Gamma} \hat{G}_E(\mathbf{k}, z, z', \omega) \frac{\hat{\varepsilon}_e - \hat{\varepsilon}_e^\dagger}{2i} \hat{G}_H^\dagger(\mathbf{k}, z, z', \omega) \right] \right\}. \end{aligned} \quad (10)$$

Comparing this expression to Eq. (3), we identify the z -position photonic transmission probability:

$$\begin{aligned} \mathcal{T}(\mathbf{k}, z, \omega) &= 4\omega \varepsilon_0 \int_{z'} \text{Re} \\ &\times \left\{ \text{Tr} \left[\hat{\Gamma} \hat{G}_E(\mathbf{k}, z, z', \omega) \frac{\hat{\varepsilon}_e - \hat{\varepsilon}_e^\dagger}{2i} \hat{G}_H^\dagger(\mathbf{k}, z, z', \omega) \right] \right\}. \end{aligned} \quad (11)$$

We note that Eq. (11) allows one to calculate the transmission probability from the emitting layer e to any position z within the receiving layer r . Thereby, the transmission probability between these two layers, $\mathcal{T}(\mathbf{k}, \omega)$, can be obtained by the difference in the one at the two boundaries of layer r .

Let us finish this section by saying that the numerical simulation for the MO three-body system we consider has shown that $\mathcal{T}_{j \rightarrow 3}(\mathbf{k}, \omega) = \mathcal{T}_{3 \rightarrow j}(\mathbf{k}, \omega)$, with $j = 1, 2$. This reciprocity of the heat flux received/emitted by slab 3 is consistent with the results reported in Ref. [48] for a linear chain of InSb nanoparticles. It is worthwhile to mention that such a reciprocity of the heat transfer in nonreciprocal many-body systems can be analytically demonstrated by using the symmetry of the magnetic group and the second law of thermodynamics, as recently shown in Ref. [72]. With this in mind, Eq. (3) can be simplified as follows:

$$\begin{aligned} \varphi_3 &= \int_0^\infty \frac{d\omega}{2\pi} \int \frac{d\mathbf{k}}{(2\pi)^2} \sum_{j=1,2} [\Theta_j(\omega, T_j) - \Theta_3(\omega, T_3)] \\ &\times \mathcal{T}_{j \rightarrow 3}(\mathbf{k}, \omega). \end{aligned} \quad (12)$$

We employ this relation to analyze the magnetic field dependence of the RHT in the system of Fig. 1, for two different choices of temperatures. The first one, analyzed in the next section, corresponds to the thermal equilibrium between slabs 2 and 3, i.e., the intermediate slab 2 purely behaving as an electromagnetic modulator [45,46]. The second choice of temperatures is determined by the steady-state condition for the heat flux across the system, for which the net flux passing through slab 2 vanishes (see Sec. V).

IV. MAGNETIC CONTROL OF HEAT FLUXES ACROSS AN INTERMEDIATE MODULATOR

We are going to first consider the net heat flux received by slab 3 due exclusively to the thermal emission from slab 1; i.e., the role of the intermediate body is only modulating the thermal photons passing through it, behaving as an electromagnetic signal modulator [45,46]. This situation can be achieved by maintaining bodies 2 and 3 at the same temperatures $T_2 = T_3 = T$, whereas for body 1 we set $T_1 = T + \Delta T$. Under this condition, there is no heat transfer between bodies 2 and 3. This, in turn, implies that $\mathcal{T}_{2 \rightarrow 3}(\mathbf{k}, \omega)$ in Eq. (9) does not play any role, so that Eq. (12) becomes

$$\varphi_3 = \int_0^\infty \frac{d\omega}{2\pi} \int \frac{d\mathbf{k}}{(2\pi)^2} [\Theta_1(\omega, T_1) - \Theta_3(\omega, T_3)] \mathcal{T}_{1 \rightarrow 3}(\mathbf{k}, \omega). \quad (13)$$

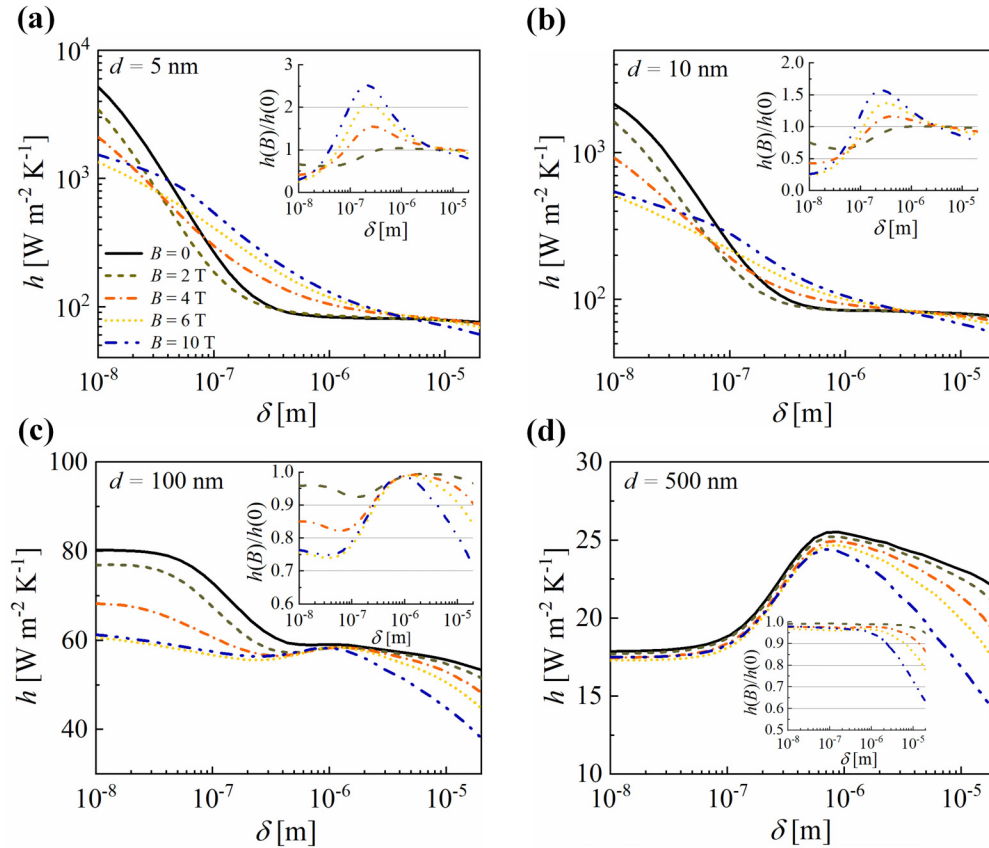


FIG. 3. Heat transfer coefficient h as a function of the intermediate slab thickness δ for different values of the external magnetic field and of the gap sizes of (a) 5 nm, (b) 10 nm, (c) 100 nm, and (d) 500 nm. The insets show the ratio between the heat transfer coefficients and their corresponding zero-field values. The temperature T is set to 300 K.

When $\Delta T \rightarrow 0$, we can introduce the linear conductance or the heat transfer coefficient h , defined as

$$h = \lim_{\Delta T \rightarrow 0} \frac{\varphi_3}{\Delta T} = \int_0^\infty \frac{d\omega}{2\pi} \int \frac{d\mathbf{k}}{(2\pi)^2} \frac{\partial \Theta(\omega, T)}{\partial T} \mathcal{T}_{1 \rightarrow 3}(\mathbf{k}, \omega). \quad (14)$$

In Fig. 3 we summarize the numerical results of the heat transfer coefficient h as a function of the intermediate slab thickness δ , varying from 10 nm to 20 μm , for several values of the magnetic field intensity B and of the gap size d . Meanwhile, to display the field effect more intuitively, we plot the ratio between the heat transfer coefficient with and without magnetic fields in the inset of each panel.

We start by discussing the main features of the heat transfer coefficient h in the absence of a magnetic field (see black solid lines in all panels of Fig. 3). By comparing the results for different gap sizes d , keeping a fixed thickness δ , one observes an expected decrease in the NFRHT as the vacuum gap overcomes the length scale for the decaying SPP's and SPhP's evanescent fields, which dominate the RHT in the near-field regime. On the other hand, a comparison of the results of panels (a)–(d) shows that the dependency of energy received by slab 3 on the thickness of the intermediate slab yields a remarkable change as d increases significantly. Specifically, in the cases of $d = 5, 10,$ and 100 nm, the heat transfer coefficients always exhibit a monotonic decline with the thickness δ [Figs. 3(a)–3(c)]. This is quite different from that observed

in Fig. 3(d), where the transfer coefficient h for a 500 nm vacuum gap has a global maximum at $\delta \approx 700$ nm. Such a maximum vanishes if d is up to the far-field value (not shown here). This peculiar transfer behavior with respect to the intermediate body size is associated with the near-field effect in macroscopic three-slab systems. In fact, as shown in Ref. [43], the intermediate slab may amplify the flux transferred from slab 1 to slab 3 when its thickness becomes comparable to the gap size (restricted to the near-field regime), as a result of the optimal coupling of the surface cavity modes occurring in vacuum gaps.

Let us turn to discussing magnetic field effects upon the energy transfer in the system under consideration. As was mentioned in the Introduction, prior studies have shown that an external static magnetic field is only responsible for reducing the NFRHT between two identical MO planar structures [23,30–32]. However, the situation becomes refreshingly different in the symmetric three-body configuration. For sufficiently small gap sizes, as $d = 5$ nm and 10 nm, the applied field decreases the heat transfer coefficient only when the intermediate slab thickness δ is close either to 10 nm or to 20 μm , as evident from the insets of Figs. 3(a) and 3(b). When d is increased to 100 nm, a field-induced reduction of the RHT arises irrespective of the thickness of slab 2, this reduction phenomenon being quite pronounced for both $\delta \approx 10$ nm and $\delta \approx 20$ μm [Fig. 3(c)]. Concerning a 500 nm gap width, the corresponding energy transfer modification is

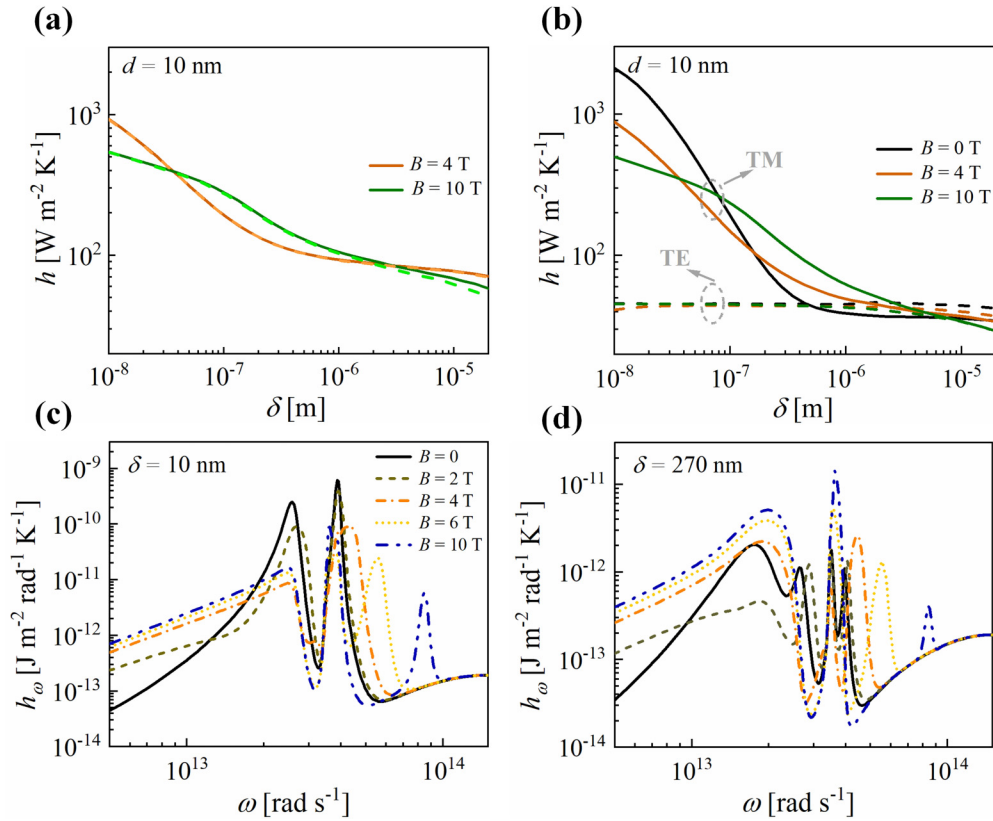


FIG. 4. (a) Heat transfer coefficient h as a function of the intermediate slab thickness δ , for magnetic field intensities of 4 and 10 T. Solid lines correspond to the results from our method considering all transmission channels, while dashed lines correspond to the ones obtained neglecting polarization conversion. (b) Heat transfer coefficient h for TE polarization (dashed lines) and TM polarization (solid lines) as a function of the thickness δ for magnetic field intensities of 0, 4, and 10 T. (c) Magnetic field effects upon the TM-polarized spectral heat transfer coefficient h_ω for $\delta = 10$ nm. (d) Same as in panel (c), but for $\delta = 270$ nm. The gap size d is 10 nm for all calculations.

appreciable only for a thicker intermediate medium, as shown in Fig. 3(d). On the other hand, we highlight that, for small gap sizes, there exists a region of values of δ , for which the presence of magnetic fields is able to enhance the NFRHT, indicating that this peculiar amplification behavior occurs in the strong near-field regime. As clearly presented in the inset of Fig. 3(a), corresponding to $d = 5$ nm, the value of $h(B)/h(0)$ can be as high as 260% at $\delta \approx 215$ nm, for a magnetic field intensity of 10 T. Incidentally, this enhancement value can be optimized by means of using a stronger external field (see Supplemental Material [71]), although such high fields are currently challenging to achieve [73]. This result marks a huge difference with respect to the case of two InSb planar slabs, implying an interplay between the HMs induced by magnetic fields and the zero-field cavity surface modes, mediated by the intermediate medium.

To elucidate the physical mechanisms behind these modifications of the NFRHT induced by magnetic fields, it is necessary to first understand the role played by polarization conversion (i.e., TM \rightarrow TE and TE \rightarrow TM). To this end, we use the analytic expression presented in Refs. [43,44] for describing the RHT in three-slab systems comprising isotropic materials to calculate the heat transfer coefficient h which neglects polarization conversion, and compare it with the results from our approach accounting for all transmission

channels (i.e., TE \rightarrow TE, TE \rightarrow TM, TM \rightarrow TM, and TM \rightarrow TE). The results for two different strengths of magnetic fields are shown in Fig. 4(a), where we take the gap size $d = 10$ nm. The good agreement between these results indicates that polarization conversion does not have a significant impact on the energy transfer. However, it should be noted that, for the high field ($B = 10$ T) and large thickness ($\delta > 1$ μ m), our Green's function approach allows us to compute exact transfer coefficients, due to the fact that the influence of polarization conversion is included. Subsequently, we further separate the TE- and TM-mode thermal contributions in Fig. 4(b), where, as a reference, the zero-field result is added. From this plot it is manifest that the modifications to the RHT occurring at $\delta < 1$ μ m can be fully attributed to the magnetic field effect upon the transmission of TM-polarized evanescent waves. On the other hand, when the thickness of the intermediate slab is pronouncedly larger than 1 μ m, the damping of the electromagnetic fields inside this slab strongly inhibit the tunneling of TM evanescent modes from slab 1 to slab 3, and therefore, the fluxes contributed by TM polarization decrease drastically until they become comparable to those contributed by TE polarization. This renders the field-induced reduction of the energy flux for TE modes comparable to that for TM modes; that is, the field-induced reduction effect is now linked to the decrease of both TE- and TM-mode contributions, distinctly

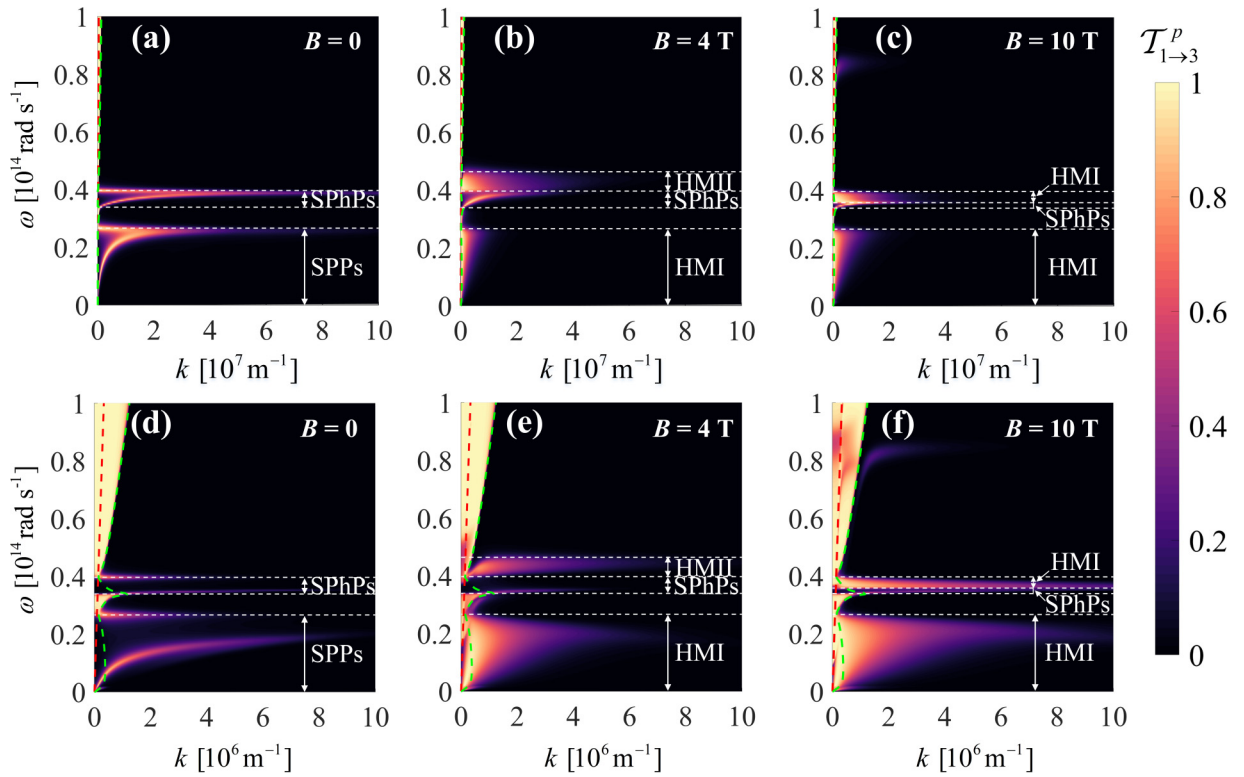


FIG. 5. Transmission probability for TM polarization from slab 1 to slab 3 as a function of the frequency ω and the parallel wave vector k for the external magnetic field $B = 4$ and 10 T. Upper (lower) panels correspond to the intermediate slab thickness $\delta = 10$ nm (270 nm). The gap size d is 10 nm. Frequency regions corresponding to surface modes (SPPs and SPhPs) and hyperbolic modes are delimited by the horizontal white dashed lines. The red (green) dashed lines correspond to vacuum (InSb); the light line $\omega = ck$ ($\omega = ck\sqrt{|\epsilon_3|}$).

different from the origin of the heat transfer reduction between two MO planar structures under the action of magnetic fields [23,30,31].

We have shown that polarization conversion does not play a significant role in the modifications of the NFRHT induced by an external magnetic field, yet the underlying physics of such modifications for TM waves, in the thickness range $\delta < 1$ μm , remains unexplained [see Figs. 3(b) and 4(b)]. For this, we now focus on the analysis of the field effect upon the TM-polarized spectral heat transfer coefficients for the thicknesses $\delta = 10$ nm and 270 nm, shown in Figs. 4(c) and 4(d), respectively. These results clearly show that the variation of energy fluxes caused by external magnetic fields is quite sensitive to the geometrical parameter of the modulator slab. Specifically, for a 10 nm intermediate slab, the applied field reduces the height of the zero-field peaks in the spectral flux associated with the SPP and SPhP modes, which is very akin to what was observed between two InSb infinite slabs [23]. In contrast, for a 270 nm thick slab, the field significantly increases the height as well as the width of the four zero-field peaks in the spectra, accounting for an effective enhancement of energy transferred to slab 3, as seen in the inset of Fig. 3(b).

These features of the spectral flux can be understood by analyzing the TM-polarized transmission probability, $\mathcal{T}_{1\rightarrow 3}^p$, shown in the upper (lower) panels of Fig. 5 for $\delta = 10$ nm ($\delta = 270$ nm), and for three different strengths of magnetic fields (i.e., $B = 0, 4,$ and 10 T). In each panel, we plot the frequency regions that support SPPs, SPhPs, and HMI and

HMI modes when InSb is exposed to the considered field strengths.

Comparing the transmission probability of Figs. 5(a) and 5(d) allows us to conclude that a very thin intermediate slab favors the formation of a zero-field cavity mode by coupling, inside of it, the evanescent fields from surface modes at the interfaces of slabs 1 and 3. This can be understood by analyzing the radiation penetration depth l . In the electrostatic limit, the penetration depth of an evanescent wave can be approximated by $l \approx k^{-1}$ [2]. Since only evanescent waves with $l \geq d$ can tunnel from slab 1 to slab 2, the largest contributing parallel wave vector k_{max} between them, holding a dominant role in the near field, can be approximated as $k_{\text{max}} \approx d^{-1}$ (a numerical proof is also provided in the Supplemental Material [71]) with an associated penetration depth $l \approx d$. Therefore, for a 10 nm intermediate slab, we have $l \approx \delta$, enabling the coupling of surface modes at the two interfaces of the intermediate slab [74]. For this reason, the high transmission zones in Fig. 5(a) follow the dispersion law of cavity modes [15]. In contrast, when the slab has a thickness of 270 nm ($\delta \gg l$), this thicker medium inhibits the coupling of the evanescent modes coming from the outermost slabs, as demonstrated by the transmission bands resembling uncoupled dispersion laws of single surfaces.

To display the influence of the intermediate slab thickness on the penetration depth of the evanescent modes more intuitively, in Figs. 6(a) and 6(b) we plot the spatial profile of the absorbed heat (for TM polarization) inside the

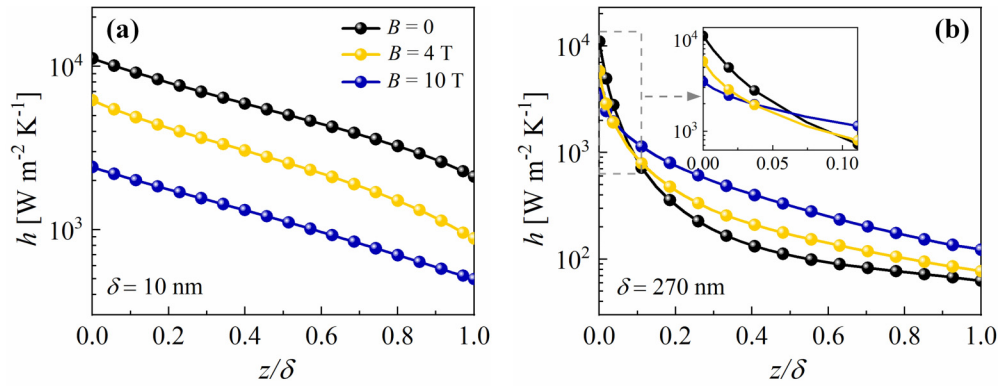


FIG. 6. Magnetic field dependence of the spatial profile of the TM-polarized energy flux across the intermediate slab with a thickness of (a) 10 nm and (b) 270 nm.

intermediate slab with $\delta = 10$ and 270 nm, respectively. It can be clearly observed that, in the absence of a magnetic field (black curves), the energy flux decays exponentially inside the 270 nm thick slab, as a result of the strong damping of the fields inside of it. Such a spatial dependence significantly differs from the convex profile of the heat flux for $\delta = 10$ nm, due to the coupled evanescent fields coming from the outermost slabs.

We next illustrate the variation of the transmission probability under the application of external magnetic fields. Figure 5 shows that, as the magnetic field increases, the HMs gradually dominate energy transfer in the considered system, and they can benefit, or not benefit, the photon tunneling, which depends on the intermediate slab thickness. Apparently, for $\delta = 10$ nm, the appearance of HMs will give rise to the destruction of the zero-field cavity mode between slabs 1 and 3. Besides, as shown in Figs. 5(a)–5(c), these field-induced HMs have significantly smaller wave-vector cutoffs relative to the disappeared surface modes, resulting in the reduced height of spectral peaks under the action of magnetic fields in Fig. 4(c). Hence, the origin of this field-induced reduction effect is the same as that found in MO two-body configurations [23,30–32]. This can be further supported by observations of Fig. 6(a). First of all, we see that, in fact, the presence of magnetic fields has strongly suppressed the energy flux by tunneling into slab 2 (corresponding to $z/\delta = 0$), especially for high fields, which is exactly due to the significant replacement of large wave-vector surface modes by those field-induced HMs with the small wave-vector cutoffs. Secondly, for such a sufficiently small thickness, the evanescent fields are weakly damped in the intermediate body (as discussed before). These two factors jointly determine that, within the intermediate slab, the energy flux at finite fields is always smaller as compared to the zero-field case [Fig. 6(a)]. Thus, one finally sees that the magnetic field reduces the transmission probability towards slab 3 due to the appearance of HMs. However, when δ is increased to 270 nm, we see in Fig. 6(b) that, in contrast to the zero field, the finite fields lead to the radiative flux inside the intermediate slab decreasing at a slower rate, although still suppressing the flux entering into the slab strongly again due to the appearance of small wave-vector HMs. This peculiar magnetic field behavior is exactly related to these HMs which have a larger penetration depth relative to the disappeared

zero-field surface modes (since $l \approx k^{-1}$). Let us recall that the evanescent fields coming from the surface modes at the interfaces of slabs 1 and 3 do not couple inside such a thick intermediate slab to form zero-field cavity modes. We thus conclude that the role of the magnetic field is now to convert a low flux tunneling, arising from the strong damping of the uncoupled surface modes inside the intermediate medium, into an efficient tunneling mediated by the propagating HMs, whose capability to propagate increases with the applied field intensity, as evidenced by the profiles of Fig. 6(b). This makes those field-induced HMs exhibit broader bands and even larger wave-vector cutoffs relative to the zero-field surface modes, as observed in Figs. 5(d)–5(f).

V. INTERMEDIATE MEDIUM PRODUCING THERMAL CONTRIBUTIONS IN STEADY STATE

In the previous section, we demonstrated that an applied magnetic field can not only reduce but also enhance the NFRHT in the simple MO three-slab configuration, associated with the interplay between the damped evanescent fields of the surface waves and the propagating hyperbolic modes induced by external magnetic fields. Notably, this discovery is achieved under the assumption of thermal equilibrium between slabs 2 and 3. Therefore, it is natural to ask if this field-induced enhancement, obtained for $d = 10$ nm and $\delta = 270$ nm, persists when the intermediate medium starts providing an additional contribution [i.e., $T_2 \neq T_3$, so that $\mathcal{T}_{2 \rightarrow 3}(\mathbf{k}, \omega)$ plays a role]. Here, from a practical point of view, we are going to consider a general steady-state situation [43,44,47]. Specifically, we assume that the external slabs 1 and 3 are still held at temperatures T_1 and T_3 , respectively, while the intermediate slab now relaxes into steady state, and thus has an equilibrium temperature T_2 . This temperature can be solved by using the thermal equilibrium condition that the net energy fluxes to and from slab 2 should be zero, i.e.,

$$\Delta\varphi = \varphi_{1 \rightarrow 2} - \varphi_{2 \rightarrow 3} = 0. \quad (15)$$

Here, $\varphi_{1 \rightarrow 2} = \int_0^\infty \frac{d\omega}{2\pi} \int \frac{d\mathbf{k}}{(2\pi)^2} [\Theta_1(\omega, T_1) - \Theta_2(\omega, T_2)] \mathcal{T}_{1 \rightarrow 2}(\mathbf{k}, \omega)$ represents the net flux from slab 1 to slab 2, while $\varphi_{2 \rightarrow 3} = \int_0^\infty \frac{d\omega}{2\pi} \int \frac{d\mathbf{k}}{(2\pi)^2} [\Theta_2(\omega, T_2) - \Theta_3(\omega, T_3)] \mathcal{T}_{2 \rightarrow 3}(\mathbf{k}, \omega)$ represents that from slab 2 to slab 3. Note that, since the

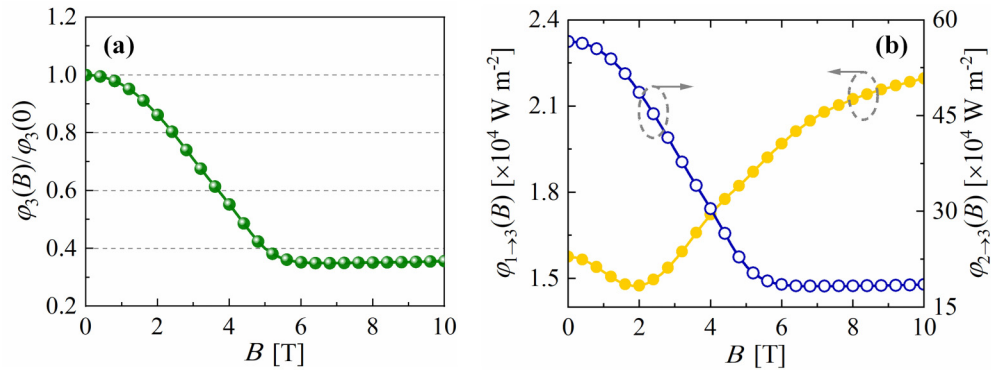


FIG. 7. (a) Total steady-state heat flux absorbed by slab 3 as a function of the magnetic field and normalized to the zero-field value. (b) Net heat fluxes $\varphi_{1\rightarrow 3}$ and $\varphi_{2\rightarrow 3}$ transferred from slabs 1 and 2 to slab 3, as a function of the magnetic field intensity. The temperatures of slab 1 and slab 3 are set to $T_1 = 400$ K and $T_3 = 300$ K, respectively. The gap size d is 10 nm, and the intermediate slab has a thickness $\delta = 270$ nm.

system under consideration is symmetric with respect to slab 2, we always have $\mathcal{T}_{1\rightarrow 2}(\mathbf{k}, \omega) = \mathcal{T}_{2\rightarrow 3}(\mathbf{k}, \omega)$, regardless of the presence of magnetic fields. Based on this, Eq. (15) can be rewritten as

$$\Delta\varphi = \int_0^\infty \frac{d\omega}{2\pi} \int \frac{d\mathbf{k}}{(2\pi)^2} [\Theta_1(\omega, T_1) + \Theta_3(\omega, T_3) - 2\Theta_2(\omega, T_2)] \times \mathcal{T}_{2\rightarrow 3}(\mathbf{k}, \omega) = 0. \quad (16)$$

From Eq. (16) it is clear that, once one determines the energy transmission coefficient $\mathcal{T}_{2\rightarrow 3}(\mathbf{k}, \omega)$ as well as the temperatures T_1 and T_3 , the equilibrium temperature T_2 can be easily solved. Note that the value of $\mathcal{T}_{2\rightarrow 3}(\mathbf{k}, \omega)$ will be changed for different strengths of the applied field. In the following we take the temperatures $T_1 = 400$ K and $T_3 = 300$ K, and assume that the optical properties of the InSb remain unchanged for 400 K.

Figure 7(a) shows the total steady-state flux received by slab 3 [given by Eq. (12)] as a function of the magnetic field intensity and normalized to its zero-field value. It can be clearly seen that there is a monotonic decrease in the energy flux with the applied field, until it saturates for fields up to above 6 T. In particular, this field-induced reduction of near-field fluxes reaches approximately 70% for $B > 6$ T, which is nearly consistent with the result for two InSb infinite slabs separated by a vacuum gap of 10 nm [23]. One thus might think that this reduction of the RHT is due entirely to the full replacement of SPP and SPhP modes by HMs. However, this is not completely true, as exhibited in Fig. 7(b), where it can be observed that the net heat fluxes from slabs 1 and 2 to slab 3 exhibit different dependences on the field intensity. More specifically, the flux $\varphi_{1\rightarrow 3}$ is increased obviously under the application of relatively high fields, consistent with the enhancement effect mediated by the intermediate slab (as illustrated in the previous section). On the other hand, the flux $\varphi_{2\rightarrow 3}$ involves the direct exchange of heat between slabs 2 and 3, for which it is not surprising to observe its rapid decrease with the applied field, referring to the case of two InSb planar slabs. Nevertheless, since slabs 2 and 3 are in closer proximity, the flux they transfer overcomes by almost an order of magnitude the one between slabs 1 and 3. Consequently, as the field intensity increases, the reduction of $\varphi_{2\rightarrow 3}$ always

dominates the increase of $\varphi_{1\rightarrow 3}$, leading to the net decreasing flux arriving at slab 3.

VI. CONCLUSIONS

In conclusion, we have theoretically investigated the magnetic field effect on the near-field heat transfer in a MO many-body system consisting of three parallel n -doped InSb slabs. We first generalized a general Green's function approach for the calculation of the RHT in many-body planar configurations made of complex anisotropic materials. Based on this approach, we showed that, when the intermediate slab acts as an electromagnetic modulator in thermal equilibrium with the cold slab, the applied magnetic field is able to either reduce or even enhance the NFRHT in the symmetric MO configuration. By analyzing thermal contributions from the thermal evanescent modes, it was further found that the mechanism of this magnetic-field-induced reduction effect can be fundamentally varied if the intermediate medium thickness yields a substantial variation; for instance, when these MO slabs are separated by a 10 nm vacuum gap, the field-induced reduction behavior occurring at small thicknesses (much smaller than 1 μm) is due exclusively to the fundamental change of TM modes, i.e., the effective replacement of zero-field surface modes by field-induced HMs, whereas the reduction behavior at relatively large thicknesses (pronouncedly larger than 1 μm) results from the joint decrease of TE- and TM-mode thermal contributions. More importantly, we demonstrated that the field-induced enhancement effect is closely related to the appearance of HMs, showing that this peculiar effect occurs when the thickness of the intermediate slab is large enough to hinder the coupling of the evanescent fields inside of it, leading to a low photon tunneling, which, in turn, may be effectively enhanced by the propagating HMs induced by fields. Finally, we also pointed out that such a field-induced enhancement of the near-field flux received by the cold slab will disappear if the whole system reaches steady state. This is because a net decrease of fluxes arriving at the cold terminal is achieved due to the additional flux it receives from the intermediate medium. Our work may inspire one to further explore the magnetic field effect upon the nanoscale RHT in more complex macroscopic many-body systems, such as periodic or aperiodic many-slab configurations.

ACKNOWLEDGMENTS

We thank I. Latella for fruitful discussions. This work was supported by the National Natural Science Foundation

of China (Grant No. U22A20210) and by the Fundamental Research Funds for the Central Universities (Grant No. FR-FCU5710094020).

-
- [1] D. Polder and M. Van Hove, Theory of radiative heat transfer between closely spaced bodies, *Phys. Rev. B* **4**, 3303 (1971).
- [2] S. M. Rytov, Y. A. Kravtsov, and V. I. Tatarskii, *Principles of Statistical Radiophysics 3* (Springer-Verlag, Berlin, 1989).
- [3] J.-P. Mulet, K. Joulain, R. Carminati, and J.-J. Greffet, Enhanced radiative heat transfer at nanometric distances, *Microscale Thermophys. Eng.* **6**, 209 (2002).
- [4] A. I. Volokitin and B. N. J. Persson, Near-field radiative heat transfer and noncontact friction, *Rev. Mod. Phys.* **79**, 1291 (2007).
- [5] R. Liu, C. Zhou, Y. Zhang, Z. Cui, X. Wu, and H. Yi, Near-field radiative heat transfer in hyperbolic materials, *Int. J. Extrem. Manuf.* **4**, 032002 (2022).
- [6] L. Rincón-García, D. Thompson, R. Mittapally, N. Agraït, E. Meyhofer, and P. Reddy, Enhancement and Saturation of Near-Field Radiative Heat Transfer in Nanogaps between Metallic Surfaces, *Phys. Rev. Lett.* **129**, 145901 (2022).
- [7] A. Narayanaswamy and G. Chen, Surface modes for near field thermophotovoltaics, *Appl. Phys. Lett.* **82**, 3544 (2003).
- [8] A. Fiorino, L. Zhu, D. Thompson, R. Mittapally, P. Reddy, and E. Meyhofer, Nanogap near-field thermophotovoltaics, *Nat. Nanotechnol.* **13**, 806 (2018).
- [9] J. Song, M. Lim, S. S. Lee, and B. J. Lee, Analysis of Photocurrent Generation Within a Schottky-Junction-Based Near-Field Thermophotovoltaic System, *Phys. Rev. Appl.* **11**, 044040 (2019).
- [10] J. DeSutter, L. Tang, and M. Francoeur, A near-field radiative heat transfer device, *Nat. Nanotechnol.* **14**, 751 (2019).
- [11] W. J. Kim, X. Vidal, A. Baev, H. S. Jee, M. T. Swihart, and P. N. Prasad, Photothermal-reaction-assisted two-photon lithography of silver nanocrystals capped with thermally cleavable ligands, *Appl. Phys. Lett.* **98**, 133110 (2011).
- [12] W. A. Challener, C. Peng, A. V. Itagi, D. Karns, W. Peng, Y. Peng, X. M. Yang, X. Zhu, N. J. Gokemeijer, Y.-T. Hsia, G. Ju, R. E. Rottmayer, M. A. Seigler, and E. C. Gage, Heat-assisted magnetic recording by a near-field transducer with efficient optical energy transfer, *Nat. Photonics* **3**, 220 (2009).
- [13] A. Kittel, W. Müller-Hirsch, J. Parisi, S.-A. Biehs, D. Reddig, and M. Holthaus, Near-Field Heat Transfer in a Scanning Thermal Microscope, *Phys. Rev. Lett.* **95**, 224301 (2005).
- [14] S.-A. Biehs, M. Tschikin, and P. Ben-Abdallah, Hyperbolic Metamaterials as an Analog of a Blackbody in the Near Field, *Phys. Rev. Lett.* **109**, 104301 (2012).
- [15] B. Song, Y. Ganjeh, S. Sadat, D. Thompson, A. Fiorino, V. Fernández-Hurtado, J. Feist, F. J. García-Vidal, J. C. Cuevas, P. Reddy, and E. Meyhofer, Enhancement of near-field radiative heat transfer using polar dielectric thin films, *Nat. Nanotechnol.* **10**, 253 (2015).
- [16] V. Fernández-Hurtado, F. J. García-Vidal, S. Fan, and J. C. Cuevas, Enhancing Near-Field Radiative Heat Transfer With Si-Based Metasurfaces, *Phys. Rev. Lett.* **118**, 203901 (2017).
- [17] J. Yang, W. Du, Y. Su, Y. Fu, S. Gong, S. He, and Y. Ma, Observing of the super-Planckian near-field thermal radiation between graphene sheets, *Nat. Commun.* **9**, 1 (2018).
- [18] J. Shen, X. Liu, and Y. Xuan, Near-Field Thermal Radiation Between Nanostructures of Natural Anisotropic Material, *Phys. Rev. Appl.* **10**, 034029 (2018).
- [19] C.-L. Zhou, L. Qu, Y. Zhang, and H.-L. Yi, Enhancement and active mediation of near-field radiative heat transfer through multiple nonreciprocal graphene surface plasmons, *Phys. Rev. B* **102**, 245421 (2020).
- [20] P. J. van Zwol, K. Joulain, P. Ben-Abdallah, and J. Chevrier, Phonon polaritons enhance near-field thermal transfer across the phase transition of VO₂, *Phys. Rev. B* **84**, 161413(R) (2011).
- [21] O. Ilic, M. Jablan, J. D. Joannopoulos, I. Celanovic, H. Buljan, and M. Soljačić, Near-field thermal radiation transfer controlled by plasmons in graphene, *Phys. Rev. B* **85**, 155422 (2012).
- [22] K. Chen, P. Santhanam, S. Sandhu, L. Zhu, and S. Fan, Heat-flux control and solid-state cooling by regulating chemical potential of photons in near-field electromagnetic heat transfer, *Phys. Rev. B* **91**, 134301 (2015).
- [23] E. Moncada-Villa, V. Fernández-Hurtado, F. J. García-Vidal, A. García-Martín, and J. C. Cuevas, Magnetic field control of near field radiative heat transfer and the realization of highly tunable hyperbolic thermal emitters, *Phys. Rev. B* **92**, 125418 (2015).
- [24] H. Wu, Y. Huang, L. Cui, and K. Zhu, Active Magneto-Optical Control of Near-Field Radiative Heat Transfer between Graphene Sheets, *Phys. Rev. Appl.* **11**, 054020 (2019).
- [25] G. Tang, J. Chen, and L. Zhang, Twist-induced control of near-field heat radiation between magnetic Weyl semimetals, *ACS Photonics* **8**, 443 (2021).
- [26] C. Zheng, G. Hu, X. Liu, X. Kong, L. Wang, and C.-W. Qiu, Molding broadband dispersion in twisted trilayer hyperbolic polaritonic surfaces, *ACS Nano* **16**, 13241 (2022).
- [27] J. C. Cuevas, and F. J. García-Vidal, Radiative heat transfer, *ACS Photonics* **5**, 3896 (2018).
- [28] R. M. Abraham Ekeroth, P. Ben-Abdallah, and J. C. Cuevas, and García-Martín, Anisotropic thermal magnetoresistance for an active control of radiative heat transfer, *ACS Photonics* **5**, 705 (2018).
- [29] A. Ott, R. Messina, P. Ben-Abdallah, and S.-A. Biehs, Magneto thermoplasmonics: From theory to applications, *J. Photonics Energy* **9**, 032711 (2019).
- [30] J. Song, Q. Cheng, L. Lu, B. Li, K. Zhou, B. Zhang, Z. Luo, and X. Zhou, Magnetically Tunable Near-Field Radiative Heat Transfer in Hyperbolic Metamaterials, *Phys. Rev. Appl.* **13**, 024054 (2020).
- [31] E. Moncada-Villa and J. C. Cuevas, Near-field radiative heat transfer between one-dimensional magnetophotonic crystals, *Phys. Rev. B* **103**, 075432 (2021).
- [32] E. Moncada-Villa and J. C. Cuevas, Magnetic field effects in the near-field radiative heat transfer between planar structures, *Phys. Rev. B* **101**, 085411 (2020).

- [33] G. Tang, L. Zhang, Y. Zhang, J. Chen, and C. T. Chan, Near-Field Energy Transfer between Graphene and Magneto-Optic Media, *Phys. Rev. Lett.* **127**, 247401 (2021).
- [34] D. K. Efimkin and A. H. MacDonald, Many-body theory of trion absorption features in two-dimensional semiconductors, *Phys. Rev. B* **95**, 035417 (2017).
- [35] S.-A. Biehs, R. Messina, P. S. Venkataram, A. W. Rodriguez, J. C. Cuevas, and P. Ben-Abdallah, Near-field radiative heat transfer in many-body systems, *Rev. Mod. Phys.* **93**, 025009 (2021).
- [36] F. Bottcher, J. N. Schmidt, M. Wenzel, J. Hertkorn, M. Y. Guo, T. Langen, and T. Pfau, Transient Supersolid Properties in an Array of Dipolar Quantum Droplets, *Phys. Rev. X* **9**, 011051 (2019).
- [37] P. Ben-Abdallah, S.-A. Biehs, and K. Joulain, Many-Body Radiative Heat Transfer Theory, *Phys. Rev. Lett.* **107**, 114301 (2011).
- [38] R. Messina, M. Tschikin, S.-A. Biehs, and P. Ben-Abdallah, Fluctuation-electrodynamics theory and dynamics of heat transfer in systems of multiple dipoles, *Phys. Rev. B* **88**, 104307 (2013).
- [39] L. Zhu and S. Fan, Persistent Directional Current at Equilibrium in Nonreciprocal Many-Body Near Field Electromagnetic Heat Transfer, *Phys. Rev. Lett.* **117**, 134303 (2016).
- [40] J. Dong, J. M. Zhao, and L. H. Hua, Near-field radiative heat transfer between clusters of dielectric nanoparticles, *J. Quant. Spectrosc. Radiat. Transfer* **197**, 114 (2018).
- [41] E. Tervo, M. Francoeur, B. Cola, and Z. M. Zhang, Thermal radiation in systems of many dipoles, *Phys. Rev. B* **100**, 205422 (2019).
- [42] J. Song, L. Lu, B. Li, B. Zhang, R. Hu, X. Zhou, and Q. Cheng, Thermal routing via near-field radiative heat transfer, *Int. J. Heat Mass Transfer* **150**, 119346 (2020).
- [43] R. Messina, M. Antezza, and P. Ben-Abdallah, Three-Body Amplification of Photon Heat Tunneling, *Phys. Rev. Lett.* **109**, 244302 (2012).
- [44] P. Ben-Abdallah and S.-A. Biehs, Near-Field Thermal Transistor, *Phys. Rev. Lett.* **112**, 044301 (2014).
- [45] R. Messina, P. Ben-Abdallah, B. Guizal, M. Antezza, and S.-A. Biehs, Hyperbolic waveguide for long-distance transport of near-field heat flux, *Phys. Rev. B* **94**, 104301 (2016).
- [46] Y. H. Kan, C. Y. Zhao, and Z. M. Zhang, Enhancement and Manipulation of Near-Field Radiative Heat Transfer Using an Intermediate Modulator, *Phys. Rev. Appl.* **13**, 014069 (2020).
- [47] N. Zolghadr and M. Nikbakht, Radiative resistance at the nanoscale: Thermal barrier, *Phys. Rev. B* **102**, 035433 (2020).
- [48] I. Latella, P. Ben-Abdallah, and M. Nikbakht, Radiative thermal rectification in many-body systems, *Phys. Rev. B* **104**, 045410 (2021).
- [49] Z. Yu, X. Li, T. Lee, and H. Iizuka, Near-field radiative heat transfer in three-body Weyl semimetals, *Opt. Express* **30**, 31584 (2022).
- [50] R. Messina and M. Antezza, Three-body radiative heat transfer and Casimir-Lifshitz force out of thermal equilibrium for arbitrary bodies, *Phys. Rev. A* **89**, 052104 (2014).
- [51] I. Latella, P. Ben-Abdallah, S.-A. Biehs, M. Antezza, and R. Messina, Radiative heat transfer and nonequilibrium Casimir-Lifshitz force in many-body systems with planar geometry, *Phys. Rev. B* **95**, 205404 (2017).
- [52] M. Krüger, G. Bimonte, T. Emig, and M. Kardar, Trace formulas for nonequilibrium Casimir interactions, heat radiation, and heat transfer for arbitrary objects, *Phys. Rev. B* **86**, 115423 (2012).
- [53] B. Müller, R. Incardone, M. Antezza, T. Emig, and M. Krüger, Many-body heat radiation and heat transfer in the presence of a non-absorbing background medium, *Phys. Rev. B* **95**, 085413 (2017).
- [54] S. Molesky, P. S. Venkataram, W. Jin, and A. W. Rodriguez, Fundamental limits to radiative heat transfer: Theory, *Phys. Rev. B* **101**, 035408 (2020).
- [55] P. Ben-Abdallah, Photon Thermal Hall Effect, *Phys. Rev. Lett.* **116**, 084301 (2016).
- [56] I. Latella and P. Ben-Abdallah, Giant Thermal Magnetoresistance in Plasmonic Structures, *Phys. Rev. Lett.* **118**, 173902 (2017).
- [57] J. Dong, S. Zhang, W. Zhang, C. Zheng, and L. Liu, Eigenmode analysis of dynamical many-body near-field radiative heat transfer mediated by an external magnetic field, *Int. J. Heat Mass Transfer* **196**, 123318 (2022).
- [58] I. Latella, S.-A. Biehs, R. Messina, A. W. Rodriguez, and P. Ben-Abdallah, Ballistic near-field heat transport in dense many-body systems, *Phys. Rev. B* **97**, 035423 (2018).
- [59] M.-J. He, Q. H., Y. Tao, W.-H. Cai, and L.-M. Ruan, Near-field radiative heat transfer in multilayered graphene system considering equilibrium temperature distribution, *Opt. Express* **27**, A953 (2019).
- [60] G. T. Papadakis, C. J. Ciccarino, L. Fan, M. Orenstein, P. Narang, and S. Fan, Deep-Subwavelength Thermal Switch via Resonant Coupling in Monolayer Hexagonal Boron Nitride, *Phys. Rev. Appl.* **15**, 054002 (2021).
- [61] M. Francoeur, M. P. Mengüç, and R. Vaillon, Solution of near-field thermal radiation in one-dimensional layered media using dyadic Green's functions and the scattering matrix method, *J. Quant. Spectrosc. Radiat. Transfer* **110**, 2002 (2009).
- [62] E. D. Palik, R. Kaplan, R. W. Gammon, H. Kaplan, R. F. Wallis, and J. J. Quinn, Coupled surface magnetoplasmon-optic-phonon polariton modes on InSb, *Phys. Rev. B* **13**, 2497 (1976).
- [63] P.-O. Chapuis, S. Volz, C. Henkel, K. Joulain, and J.-J. Greffet, Effects of spatial dispersion in near-field radiative heat transfer between two parallel metallic surfaces, *Phys. Rev. B* **77**, 035431 (2008).
- [64] A. Narayanaswamy and G. Chen, Thermal near-field radiative transfer between two spheres, *Phys. Rev. B* **77**, 075125 (2008).
- [65] B. Czaplá and A. Narayanaswamy, Near-field thermal radiative transfer between two coated spheres, *Phys. Rev. B* **96**, 125404 (2017).
- [66] S. Edalatpour and M. Francoeur, The thermal discrete dipole approximation (T-DDA) for near-field radiative heat transfer simulations in three-dimensional arbitrary geometries, *J. Quant. Spectrosc. Radiat. Transfer* **133**, 364 (2014).
- [67] L. P. Walter, E. J. Tervo, and M. Francoeur, Near-field radiative heat transfer between irregularly shaped dielectric particles modeled with the discrete system Green's function method, *Phys. Rev. B* **106**, 195417 (2022).
- [68] A. Narayanaswamy and Y. Zheng, A Green's function formalism of energy and momentum transfer in fluctuational electrodynamics, *J. Quant. Spectrosc. Radiat. Transfer* **132**, 12 (2014).

- [69] H. Chalabi, E. Hasman, and M. L. Brongersma, Near-field radiative thermal transfer between a nanostructured periodic material and a planar substrate, *Phys. Rev. B* **91**, 014302 (2015).
- [70] B. Caballero, A. García-Martín, and J. C. Cuevas, Generalized scattering-matrix approach for magneto-optics in periodically patterned multilayer systems, *Phys. Rev. B* **85**, 245103 (2012).
- [71] See Supplemental Material at <http://link.aps.org/supplemental/10.1103/PhysRevB.107.205405>, which includes Refs. [23,70], for the derivation of the electric and magnetic Green's functions, the realization of the optimal NFRHT enhancement via strong magnetic fields, and the calculation of the largest contributing wave vector from slab 1 to slab 2.
- [72] C. Guo and S. Fan, Theoretical constraints on reciprocal and non-reciprocal many-body radiative heat transfer, *Phys. Rev. B* **102**, 085401 (2020).
- [73] B. Bernáth, P. Gogoi, A. Marchese, D. Kamenskyi, H. Engelkamp, D. Arslanov, B. Redlich, P. C. M. Christianen, and J. C. Maan, Nonlinear terahertz transmission spectroscopy on Ga-doped germanium in high magnetic fields, *Phys. Rev. B* **105**, 205204 (2022).
- [74] M. Francoeur, M. P. Mengüç, and R. Vaillon, Coexistence of multiple regimes for near-field thermal radiation between two layers supporting surface phonon polaritons in the infrared, *Phys. Rev. B* **84**, 075436 (2011).